AIP | Applied Physics Letters

Phase-sensitive imaging of cold atoms at the shot-noise limit

P. S. Light, C. Perrella, and A. N. Luiten

Citation: Appl. Phys. Lett. **102**, 171108 (2013); doi: 10.1063/1.4803703
View online: http://dx.doi.org/10.1063/1.4803703
View Table of Contents: http://apl.aip.org/resource/1/APPLAB/v102/i17
Published by the AIP Publishing LLC.

Phase-sensitive imaging of cold atoms at the shot-noise limit

P. S. Light,[1,2,a)] C. Perrella,[1,2] and A. N. Luiten[1,2]
[1]*School of Physics, The University of Western Australia, Perth, WA 6009, Australia*
[2]*Institute for Photonics and Advanced Sensing (IPAS) and School of Chemistry and Physics, The University of Adelaide, Adelaide, SA 5005, Australia*

(Received 21 December 2012; accepted 18 April 2013; published online 30 April 2013)

We demonstrate simultaneous phase and amplitude imaging of cold atoms using an intrinsically stable interferometer based on polarization beam-displacers. This method allows for the straight-forward retrieval of absorption and phase-shift experienced by an optical probe transmitted through an atomic sample. Furthermore, we show that our technique has a signal-to-noise ratio limited only by photon shot-noise. © *2013 AIP Publishing LLC*. [http://dx.doi.org/10.1063/1.4803703]

Imaging and spectroscopy are two crucial, but usually separate, diagnostic tools that are frequently used to probe cold matter. Imaging provides spatially resolved information on the light scattering which can be interpreted in terms of a density distribution or other spatial structures. Sequences of images can be used to estimate temperature and atomic coherence.[1,2] On the other hand, spectroscopy can be used to derive the frequency dependent absorption and dispersion of a sample, which provides an alternative means to estimate the velocity distribution[3] or frequency shifts[4] through coupling to the environment. Ideally, one would like a technique that could do both simultaneously as one could then explore, e.g., spatial variations of the refractive index of the sample. In this letter, we experimentally demonstrate just such a scheme.

Imaging can be split into a number of variants: absorption or fluorescence imaging uses a probe beam tuned close to a strong resonance in the atoms or molecules, while a second class of imaging methods make use of an off-resonant probe beam to detect the interaction by the phase-shift acquired in transmission through the atomic sample. While, at first sight, phase-based techniques may appear less-destructive than those based on absorption, it has been shown that for optically thin atomic clouds, the maximum possible signal-to-noise ratio, for a given number of absorbed photons (and hence the level of disturbance to the system) is the same for both absorption and single-pass phase imaging.[5,6] However, in the case of optically thick samples, phase imaging can indeed be less destructive than absorption imaging.[5,6] On the other hand, spectroscopic techniques, such as frequency modulation spectroscopy,[7] can measure the transmitted phase through a cold sample with great precision, but cannot easily be applied to imaging because the transmitted light needs to be detected synchronously at each detection point with a local oscillator.

Nonetheless, due to the great interest in this field, there have been a number of attempts to build phase-sensitive imaging systems based on traditional optical techniques. Dark-ground imaging[8] and phase-contrast imaging[9] make use of masks that must be critically positioned in the Fourier plane of an imaging lens. Spatial heterodyne imaging[10] makes use of a strong reference beam and a weak tilted probe beam to produce fringes on a CCD camera. This is combined with Fourier transform techniques to retrieve the image. Diffraction contrast imaging[11] can obtain a column-density image by analyzing the diffraction of a probe beam, where Fourier transform algorithms are again used to retrieve the phase map.

An interesting recent alternative, demonstrated for imaging a single trapped ion,[12] is to take a series of images of the transmitted light at a number of planes near the image plane and determining the phase of scattered wave through its interference with the incident wave. Recently, a theoretical proposal for direct phase-shifting interferometry was given in Ref. 13. Similarly to the method just described, this technique requires multiple images taken with a number of known phase-shifts in the reference arm. It is possible to retrieve the transmitted phase from this sequence of images although, naturally, the technique requires the imaged object to be stable over the duration of the exposures. In contrast, our method requires just a single exposure, and thus avoids this constraint.

In this letter, we demonstrate the phase imaging of cold-atom clouds through the use of a polarization-based interferometer. Our technique has the advantages of both a simple optical setup and straightforward retrieval of the phase (or absorption) image.

The optical setup is shown in Fig. 1. An interferometer is formed by a pair of calcite beam-displacers, followed by a Wollaston prism used as a polarization analyzer. The first beam displacer produces spatially parallel, and orthogonally polarised, reference and probe beams. The linear polarization of the input beam to this beam displacer is set to provide equal power in the probe and reference beams. The beams are aligned such that only the probe beam traverses the atomic cloud although both beams pass through the vacuum chamber and the same optical windows. The path length difference between the probe and reference arms is adjusted to be $(n + 1/2)\lambda$ such that the two output beams from the Wollaston prism analyzer are of equal power, in the absence of the atom cloud. Any phase shift induced in transmission through the cloud will alter the power balance. This polarisation interferometer delivers a very high level of passive stability because to first order movement of the optical components causes no change in output.

The powers at the output of the Wollaston prism are given by

[a)]Electronic mail: philip.light@adelaide.edu.au

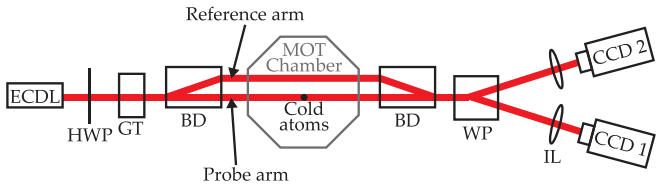

FIG. 1. Schematic of the imaging set up. GT: Glan-Taylor polarizer; BD: calcite beam displacer; HWP: half-wave plate; WP: Wollaston prism; IL: imaging lens; ECDL: external-cavity diode laser.

$$P_A = \frac{1}{4}P_0[1 + T^2 + 2T\sin\phi], \tag{1a}$$

$$P_B = \frac{1}{4}P_0[1 + T^2 - 2T\sin\phi], \tag{1b}$$

where T and ϕ are, respectively, the transmission and phase-shift through the probe arm, and P_0 is the total imaging beam power. The phase-shift and transmission of the probe arm can thus be retrieved using the following equations:

$$T = \sqrt{2(P_A + P_B)/P_0 - 1}, \tag{2a}$$

$$\phi = \sin^{-1}\left[\frac{(P_A + P_B)/P_0}{T}\right]. \tag{2b}$$

Equation (2b) shows that phase shifts of between $-\pi/2$ and $\pi/2$ can be determined without ambiguity. T and ϕ can be related to refractive index, n, through $T = \exp(-(\lambda/8\pi)\,\Im(n)L)$ and $\phi = 2\pi(L/\lambda)\Re(n)$. The two-level atom approximation gives the detuning-dependent refractive index of the cloud[11]

$$n = 1 + \rho(r)\frac{\sigma_0\lambda}{4\pi}\frac{i - 2\Delta}{1 + 4\Delta^2}, \tag{3}$$

where σ_0 is the resonant cross-section, and Δ is the detuning from resonance in units of natural line-width, Γ. $\rho(r)$ is the number density of atoms as a function of radial distance, r, from the center of the cloud. The column refractive index experienced by the probe beam is given by $\int \rho(r)dz$, which has a Gaussian distribution in the transverse plane due to the Gaussian density distribution of the atomic cloud.

We demonstrate our technique by imaging a cloud of cold ^{85}Rb atoms produced in a magneto-optical trap (MOT). The cloud consists of 4×10^8 atoms. The 1.7 mm, 0.5 μW ($\approx 0.005 I_{sat}$) imaging beam is delivered via optical fiber. A Glan-Taylor polarizer is positioned after the fiber collimation optic to impose the correct polarization at the input to the first beam displacer. The imaging beam remains on throughout the experiment.

In order to allow imaging of the atomic sample, the two output beams are incident on separate CCD cameras (Point Grey Chameleon CMLN-13S2M; 0.5 quantum efficiency). Identical 175 mm imaging lenses are used to form an image of the atom cloud at each camera, with the lens positioned to provide a magnification of 0.42.

We perform the imaging while scanning the imaging beam frequency across all hyperfine levels of the $5^2S_{1/2}$ $(F = 3) \rightarrow 5^2P_{3/2}$ (D2) transition, with a maximum detuning from resonance of 12Γ.

For each imaging frequency, three pairs of images are acquired: (a) with the cold-atoms trapped (i.e., with the MOT cooling beams and magnetic field gradients present); (b) 1 ms after the atoms are released from the trap (cooling beams and magnetic fields switched off); and (c) reference images 500 ms after release at which time the number of cold atoms still present within the probe beam is insignificant. The reference frame allows correction for changes in imaging beam power with frequency. We note that the MOT repumper beam remained on throughout the imaging process.

The total cycle time to reload the MOT and acquire the images for each imaging frequency is 2.5 s. To perform imaging with suitable resolution ($\sim$1.5 MHz) across the D2 transition thus takes $\sim$400 s. We found that the interferometer was sufficiently stable over this time scale that we could avoid any requirement for active stabilization of the arm lengths.

Imaging beam powers were chosen to allow for a 1 ms CCD exposure time, minimizing the captured fluorescence in the case where the cooling beams were on during imaging. This restriction could be lifted by imaging using the D1 transition at 795 nm and then using an interference filter to reject the 780 nm fluorescence due to the cooling beams.

Fig. 2 shows an example pair of images obtained by the CCD cameras, in this case with the imaging beam blue-detuned $\Gamma/2$ from the $5^2S_{1/2}$ $(F = 3) \rightarrow 5^2P_{3/2}$ $(F' = 4)$ cooling transition. The length scale indicated on these images is expressed in the transverse plane positioned at the atom cloud.

To convert the measured intensity data into absorption and phase shift, we start by aligning the two images by finding the beam centre of each image from the two reference frames. We do this by fitting a 2D Gaussian function to create a mapping function between the pixels on the two CCDs. We can then choose to analyze the data in two ways (we present both in this paper): either by considering the average phase-shift and absorption over a particular region of the image to obtain the change in these parameters with imaging beam frequency (see Fig. 3) or by analyzing the CCD image data at a single frequency to obtain an image of the column phase-shift and absorption (see Fig. 4).

As an example of the first analysis approach, we obtain a smoothed representation of the phase-shift and absorption at the densest part of the atomic cloud by totalling the pixel values in a 10×10 pixel region of each image (as indicated by

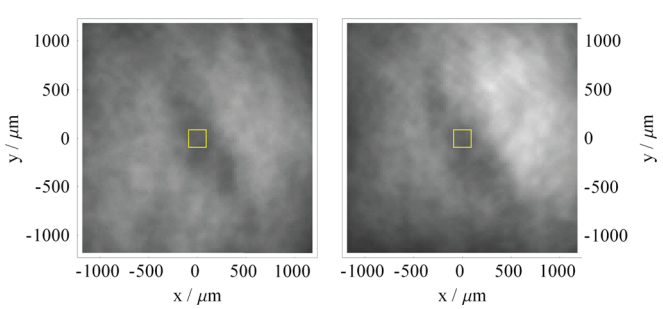

FIG. 2. Images of a cold-atom cloud obtained on the two CCD cameras for a imaging beam frequency detuning of $\Gamma/2$. The yellow boxes indicate the region of each image averaged to measure phase-shift and absorption as a function of optical imaging frequency in Fig. 3.

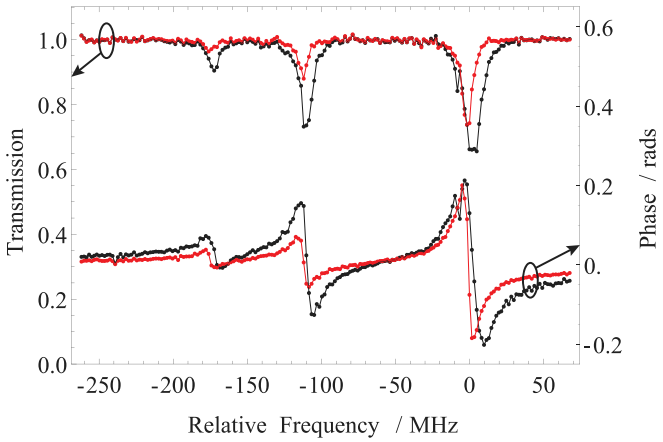

FIG. 3. Retrieved transmission (upper curves) and phase (lower curves) as a function of imaging beam frequency detuning from the $5^2S_{1/2}\,(F=3) \rightarrow 5^2P_{3/2}\,(F'=4)$ transition in ^{85}Rb. Analysis is with atoms trapped in the magneto-optical trap (black curves) and 1 ms after release of the atoms (red/grey curves).

the box in Fig. 2). For each set of cloud and reference images, the phase and absorption are retrieved using Eq. (2). The total incident power, P_0, is obtained by summing the two reference images. Fig. 3 displays the retrieved absorption and phase as a function of imaging beam frequency detuning, both with the cold atoms trapped in the magneto-optical trap (black curves) and after release of the atoms (red curves). The dispersive phase shift features associated with each of the three allowed hyperfine transitions are clearly resolved. The released atoms show smaller absorption and phase shift of the imaging beam due to the expansion and rarefaction of the cloud. The linewidth of the strongest transition for the released atoms is measured to be 6.2 ± 0.1 MHz, in agreement with the natural linewidth. The captured atoms show a shift of 3.4 MHz to higher frequency compared with the released atoms. This is in agreement with dressed-atom theory associated with the strong optical fields in the MOT.[14]

The narrow feature at the cooling laser frequency (~9 MHz red-detuned from the $5^2S_{1/2}\,(F=3) \rightarrow 5^2P_{3/2}\,(F'=4)$ transition), which is seen in both the absorption and phase profiles of the trapped atoms (black curves in Fig. 3) has been explained as a stimulated Raman process between Zeeman states of the MOT.[15] The distance between the peaks of this feature is 1.2 MHz for our experimental conditions. An approximate analysis following Souther *et al.*[16] predicts a peak spacing of ≈400 kHz due to light fields alone, with the rest of the width associated with Zeeman shifts, estimated to be up to ≈0.9 MHz due to the spatial extent of the cold atoms in the trapping magnetic field.[16]

Images of the complex transmittance can also be retrieved for the entire atomic cloud by applying Eq. (2) for each spatially matched pixel in the pair of CCD images obtained at each frequency. The result of this analysis is shown in Fig. 4, which plots absorption and phase shift as a function of displacement from the center of the atom cloud under three different imaging frequency conditions: (a) red-detuned by $\Gamma/2$; (b) on-resonance; and (c) blue-detuned by $\Gamma/2$. The phase in the reference images (nominally zero) has been calculated and subtracted from the retrieved phase in these results. This is necessary because the MOT chamber windows through which the probe and reference beams travel are not optically flat. This results in spatially varying phase changes (~0.4 rads peak-to-peak) over the cross-section of the probe and reference beams. The plots down the right-hand side of Fig. 4 clearly show the variation in atom density throughout the cloud, and its variation as a function of detuning. The sequence of plots in the left-hand

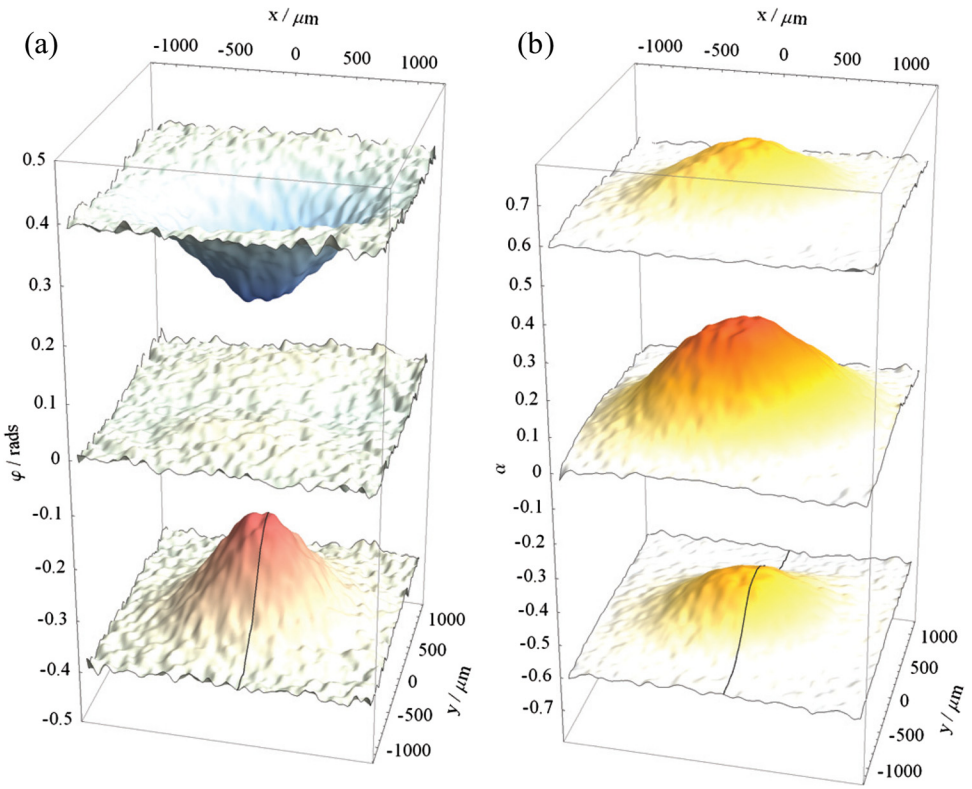

FIG. 4. Reconstructed (a) phase and (b) absorption at three different values of imaging beam frequency detuning from the $5^2S_{1/2}\,(F=3) \rightarrow 5^2P_{3/2}\,(F'=4)$ transition: $\Gamma/2$ red-detuned (top), on resonance (middle), and $\Gamma/2$ blue-detuned (bottom). The dimensions given are for the object plane of the imaging system. Detuned data are offset by $\phi = \pm 0.4$ and $\alpha = \pm 0.6$.

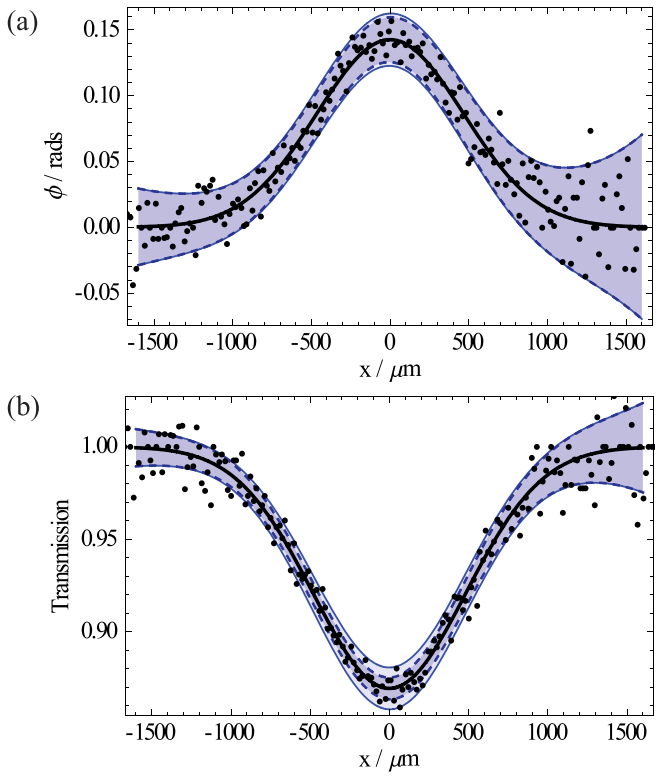

FIG. 5. Retrieved phase (a) and transmission (b) for a line profile through a single image. The black curves are Gaussian fits to the data, the dashed blue curves represent the calculated one-sigma error bounds due to photon shot-noise, and the solid blue curves show the calculated one-sigma error due to both photon shot-noise and atom shot-noise.

side of Fig. 4 shows the spatial phase variation. As expected (Eq. (3)), the phase-shift is proportional to cloud density and shows a dispersive dependence on detuning. A 2D Gaussian fit to the on-resonance absorption data gives a $1/e^2$ cloud diameter of 2.00 ± 0.02 mm.

The noise in the retrieved phase and absorption observed in the images in Fig. 4 are consistent with that expected due to shot-noise. To illustrate this, Fig. 5 plots line profiles through a single red-detuned image of Fig. 4 (taken at the position indicated by the black lines). In Fig. 5, the black curves are Gaussian fits to the data, representing the spatial distribution of the Rb atoms. The dashed blue curves represent the estimated 1σ uncertainty due to photon shot noise, taking into account both the retrieval process and the spatial variation in imaging beam intensity. The solid blue curves also include the contribution to uncertainty due to atom-number shot-noise. The asymmetry in the uncertainty curves is due to the small spatial separation between the atomic density maximum and imaging beam power maximum. We calculate that, in our experimental conditions, the shot-noise corresponds to between 0.016 rads and 0.028 rads (for $|\phi| < 0.2$ and $T > 0.7$) in the center of each image, where the imaging beam intensity is highest. The error in retrieved absolute absorption associated with shot-noise is 0.01, with only a small dependence on the absolute absorption.

When imaging the densest region of the atom cloud, $\approx$150 atoms contribute to the signal at single CCD pixel, and the photon shot-noise and atom-number shot-noise contributions are comparable under our experimental conditions. In the wings of the cloud, the number of atoms sampled decreases and photon shot-noise dominates.

The critical factor in determining the photon shot-noise is the well-depth of the CCD cameras: this parameter sets the maximum number of photons that can be detected before saturation. The cameras in this experiment had a well-depth of $\approx$16000 photoelectrons, corresponding to a maximum incident energy of $\approx$32 000 photons (after accounting for quantum efficiency). In order to lower the effect of shot noise in the image, it is necessary to collect a greater number of photons. Since the ratio of well-depth to pixel-area is nearly constant for all CCD chips, the important criteria in determining the maximum number of photons is the total image sensing area rather than either the number of pixels or well-depth. Increasing the CCD sensor diagonal size from 1/3″ to 1″, together with an equivalent increase in probe power, would allow a 9-fold increase in collected photons, without the need to increase integration time. Together with optimizing the imaging optics to better fill the CCDs with the cold-atom images, we estimate that the noise observed in our results could be reduced by an order of magnitude.

In Fig. 5, we have used just a single image for the noise analysis. It should be noted that for Fig. 3 the data at each probe frequency are obtained from an independent atomic cloud and thus the noise observed here should be due to both shot-noise as well as the imperfect reproducibility of the atomic cloud. For this reason, the data do not show the full $\sqrt{100}$ improvement in noise that would otherwise be expected due to averaging over a 10×10 pixel region, although, it does show a factor of 5 improvement which emphasises the reasonably high degree of atom cloud reproducibility of our MOT apparatus.

Our results demonstrate a cold-atom imaging technique based on an intrinsically stable interferometer that can simultaneously retrieve both absorption and phase-shift images of the cloud. We believe that the simplicity of the optical setup and straightforward retrieval of phase-shift will allow such a scheme to be widely implemented.

We thank Alexander Akoulchine for bringing the stimulated Raman process to our attention, and Tom Stace for assistance in consideration of atomic shot noise. We would like to thank the Australian Research Council for supporting this work under Grant Nos. DE120102028, DP0877938, and FT0991631.

[1]D. Miller, J. Anglin, J. Abo-Shaeer, K. Xu, J. Chin, and W. Ketterle, Phys. Rev. A **71**, 043615 (2005).
[2]K. Madison, F. Chevy, W. Wohlleben, and J. Dalibard, Phys. Rev. Lett. **84**, 806 (2000).
[3]M. Brzozowska, T. Brzozowski, J. Zachorowski, and W. Gawlik, Phys. Rev. A **73**, 063414 (2006).
[4]T. Brzozowski, M. Brzozowska, J. Zachorowski, M. Zawada, and W. Gawlik, Phys. Rev. A **71**, 013401 (2005).
[5]J. Hope and J. Close, Phys. Rev. Lett. **93**, 180402 (2004).
[6]J. Hope and J. Close, Phys. Rev. A **71**, 043822 (2005).
[7]V. Savalli, G. Z. Horvath, P. D. Featonby, L. Cognet, N. Westbrook, C. I. Westbrook, and A. Aspect, Opt. Lett. **24**, 1552 (1999).
[8]M. Andrews, M. Mewes, N. van Druten, D. Durfee, D. Kurn, and W. Ketterle, Science **273**, 84 (1996).
[9]M. Andrews, D. Kurn, H. Miesner, and D. Durfee, Phys. Rev. Lett. **79**, 553 (1997).

[10]S. Kadlecek, J. Sebby, R. Newell, and T. G. Walker, Opt. Lett. **26**, 137 (2001).
[11]L. Turner, K. Domen, and R. Scholten, Phys. Rev. A **72**, 031403 (2005).
[12]A. Jechow, B. G. Norton, S. Händel, V. Blüms, E. W. Streed, and D. Kielpinski, Phys. Rev. Lett. **110**, 113605 (2013).
[13]T. Ku, C. Huang, and B. Shiau, Opt. Express **19**, 3730 (2011).
[14]M. Mitsunaga, T. Mukai, K. Watanabe, and T. Mukai, J. Opt. Soc. Am. B **13**, 2696 (1996).
[15]D. Grison, B. Lounis, C. Salomon, J. Courtois, and G. Grynberg, Europhys. Lett. **15**, 149 (1991).
[16]N. Souther, R. Wagner, P. Harnish, M. Briel, and S. Bali, Laser Phys. Lett. **7**, 321 (2010).